JURNAL KARTIKA KIMIA

J. Kartika Kimia, Mei 2024, 7, (1), 40-49
Journal homepage: http://jkk.unjani.ac.id/index.php/jkk
P-ISSN: 2655-1322 E-ISSN: 2655-0938

Synthesis and Characterization of Calcium Oxide Nanoparticles and Their Application in the Adsorption of Indigo Carmine

Brigitta Stacia Maharani[1], Fitri Khoerunnisa[1,*], Budiman Anwar[1], Hendrawan[1], Ida Hamidah[2], Mita Nurhayati[1,2], Eli Hendrik Sanjaya[3]
[1]Department of Chemistry, Universitas Pendidikan Indonesia, Setiabudi 229 Bandung 40154, Indonesia
[2]Department of Engineering, Universitas Pendidikan Indonesia, Setiabudi 229 Bandung 40154, Indonesia
[3]Department of Chemistry, Universitas Negeri Malang, Malang 90222, Indonesia
*E-mail: fitri@upi.edu

DOI: https://doi.org/10.26874/jkk.v7i1.253

Received: 21 Oct 2023, *Revised*: 12 June 2024, *Accepted*: 12 June 2024, O*nline*: 12 June 2024

Abstract

This research aims to determine the optimum conditions for the synthesis of CaO nanoparticles using the coprecipitation method, determine the characteristics of the CaO nanoparticles synthesized, and determine the effect of the performance of CaO nanoparticles as an adsorbent for indigo carmine dyes. CaO nanoparticles were successfully synthesized using the coprecipitation method at the optimum conditions of 1 M NaOH concentration and formation temperature of 400+200°C with the highest % yield reaching 74.56%. The successful formation of CaO nanoparticles was proven by the appearance of a 2-theta diffraction peak of 23.12°; 39.2°; 57.9°; and 67.2° which is identical to the lattice structure of CaO with hkl indices (200), (311), (422) and (600) and a crystal size of up to 4.96 nm. SEM images support the formation of CaO nanoparticles with an average particle size of 98.1 nm and a varying size distribution. The IR spectrum of the formation of CaO nanoparticles with the appearance of Ca-O peaks at wavelengths of 3640, 1400, 860, and 791 cm^{-1}. The adsorption capacity of indigo carmine on CaO nanoparticles was greatest at an adsorbent dose of 10 mg, adsorbate concentration of 100 ppm and a contact time of 50 minutes. The most appropriate adsorption isotherm model and adsorption kinetics model was the Koble-Corrigan model and the pseudo second order model, respectively.

Keywords: adsorption, calcium oxide, indigo carmine, isotherm, nanoparticle

1 Introduction

Wastewater can be generated from various sources such as households, industry, and other public places, that is harmful to living things. Some undesirable substances in wastewater can be the main cause of contamination in the water, soil, and air environment [1]. Recently, a very rapid increase in the textile industries in Indonesia up to 10.45% is of a great challenge in term of industrial waste management due to [2], larger water consumption for various wet processing procedures, specifically, various of chemicals for instance acids, alkaline, dyes, hydrogen peroxide, starch, surfactants, dispersing agents and metal-based soaps are found in the textile industry wastewater [3].

Many types of commercial dyes are commonly used in textile industry processes. such as direct dyes, process dyes, reactive dyes, and other dyes [4]. Most of them are carcinogenic, toxic and resistant to decomposition by microbial action [5]. One of the synthetic organic dyes with acidic properties that can cause pollution to aquatic ecosystems is indigo carmine. Indigo carmine has been used for more than two centuries because of its promising coloring ability on textile materials, especially denim fabric [6].

However, the use of synthetic textile dyes creates new challenges because the waste is difficult to decompose naturally. The textile dye wastewater must be treated before it is discharged into the aquatic environment [7], since it causes dangerous pollution and eutrophication with undesired byproducts such as oxidation reactions, hydrolysis, or other chemical reactions as well as the harmful effect to human and living organisms [8].

Among wastewater treatment technologies, adsorption is considered as one of effective methods for dyes removal. In particular, the use of metal oxide nanoparticle as adsorbents [9,10] becomes promising due to its distinctive properties for instance higher aspect ratio, nanoscale size, outstanding optical, electrical, and magnetic properties [11]. Several studies report that calcium oxide nanoparticles (CaO NPs) can be used as adsorbents for various dye solutions such as coralene dark red [12], basic red 46 [13], acid blue 9 [14], and neutral red [15].

To date, the investigation on the effect of precursor concentrations on the synthesis and characteristics of CaO NPs. The concentration ofprecursor's solution essentially determines the reaction rate in nanoparticle synthesis owing to the improved collision frequency between the two reactants. The higher concentration the more collisions will occur [16]. Moreover, the application of CaO NPs in adsorption of indigo carmine (IC) dye discharged from textiles, pharmaceuticals and medicine industry is merely reported [17].

Therefore, this study aims to synthesis and to characterize CaO NPs under various conditions. In particular, the synthesis of CaO NPs was carried out by mean of hydrothermal method. The synthesized CaO NPs was characterized by X-ray diffraction techniques, FTIR spectroscopy, and scanning electron microscopy. Furthermore, adsorption studies of IC dyes in wastewater on CaO NPs was systematically conducted.

2 Method

2.1 Materials

All reagents and chemicals used are of analytical grade (99.5%). Calcium chloride anhydrous ($CaCl_2$), sodium hydroxide (NaOH), and indigo carmine dye ($C_{16}H_8N_2Na_2O_8S_2$) were purchased from Merck, Germany, used as received without any further treatment. Deionized water is used throughout all experiments.

2.2 Procedures

A total of 100 mL of 0.5 M $CaCl_2$ and 100 mL of NaOH at different concentrations of 0.5 M; 0.8 M; 1 M were used. The $CaCl_2$ and NaOH solutions were heated at 80°C. A The $CaCl_2$ solution was dropped gradually into NaOH solution under stirring (1000 rpm) until homogeneous suspension obtained. Hereafter, the suspension was centrifuged at 11,000 rpm and followed by washing using distilled water until reach pH neutral. The wet solids were collected and dried at 100°C. The dried solid was grinded and then heated using furnace at 400°C. The synthesized CaO NPs were denoted as CaO 10; CaO 8; CaO 5 correspond to variation in NaOH concentration of 1 M; 0.8 M; and 0.5 M, respectively. Apart from that, there are also CaO nanoparticles with additional temperature (400+ 200°C) which are called CaO 10'. The yield percentage (%) of synthesized CaO NPs at various NaOH solution concentrations was calculated using Equation (1), where W_o and W_t as the mass of CaO NPs in grams before and after heating using a furnace, respectively.

$$Yield(\%) = \frac{Wo-Wt}{Wo}\ x\ 100 \qquad (1)$$

2.3 Characterization of CaO NPs

The structure and functional groups of CaO NPs were characterized by FTIR spectroscopy (FTIR-Shimadzu DTG 60H) at a wavelength of 4000-400 cm^{-1}. The lattice structure and crystallinity of CaO NPs were examined by Powder X-ray Diffraction (XRD) (PANalytical Type X'Pert PRO Pw 3040/xo, Netherlands) at 40 kV and 40 mA for monochromatized Cu Kα (λ=1.5418 Å) radiation. Scanning Electron Microscopy (SEM) measurements were carried out on a Gemini 300 (ZEISS, German) SEM at magnification 5,000x and 10,000x to investigate the morphology of CaO NPs.

2.4 Adsorption Study in Indigo Carmine

The performance test of CaO nanoparticles (NPs) was conducted by preparing a stock solution of 500 mg indigo carmine (IC) in 1 liter of distilled water. Batch adsorption experiments were performed using 10, 20, 30, and 40 mg of CaO NPs placed in IC solution with a concentration of 100 ppm in a dark glass bottle at neutral pH. The adsorption isotherm study was conducted with IC solution concentrations of 10, 30, 50, 80 and 100 ppm. All mixtures were stirred mechanically, then centrifuged at 11,000 rpm. The equilibrium concentration of IC was determined spectrophotometrically at a maximum wavelength (λ_{max}) of 322 nm using a Shimadzu UV-Mini 1240 spectrophotometer.

Kinetic studies were carried out with an IC concentration of 30 ppm over a period of 1 to 60 minutes (at 10-minute intervals). The amount of IC adsorbed on the CaO surface in each experiment was calculated using Equation (2) [18]

$$Q_e = \frac{(C_0 - C_e)V}{m} \qquad (2)$$

Where Q_e is the adsorption capacity at equilibrium, Q_t is the adsorption capacity at a specific time (mg/g), C_0 is the initial concentration (mg/L), C_e or C_t is the equilibrium concentration at a specific time (mg/L), m is the mass of the adsorbent (g), and V is the volume of the solution (L).

3 Result and Discussion

3.1 Structure and Crystallinity

The X-ray diffraction technique is useful for providing information on the lattice structure and crystallinity of CaO nanoparticles [19]. Figure 1 shows the X-ray diffractogram of CaO NPs synthesized at various NaOH concentrations. The obtained diffractograms were compared with the JCPDS CaO No. 00-004-077 [20] and JCPDS $Ca(OH)_2$ No. 72-0156 [21]. Specifically, the CaO NPs synthesized at 400 + 200°C (CaO 10') exhibit typical diffraction peaks at 23.15°, 39.2°, 57.9°, and 67.2°, corresponding to the Bravais lattice planes (200), (311), (422), and (600), respectively. These peaks are in good agreement with the JCPDS CaO data. However, three peaks in diffractogram (C) corresponding to the $Ca(OH)_2$ lattice structures (001), (111), and (103) at 2θ 18.2°, 54°, and 65° still appeared.

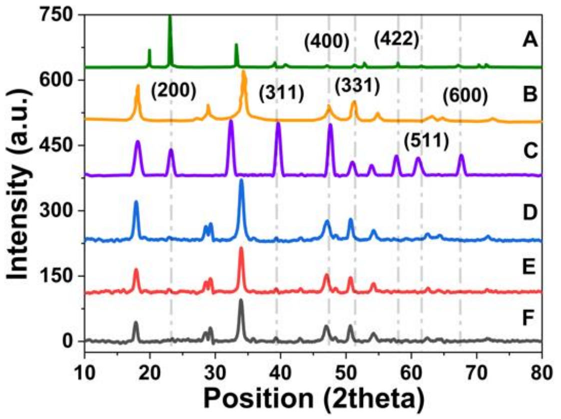

Figure 1. X-Ray Diffractogram of CaO NPs: (A) CaO from JCPDS No. 00-004-077; (B) $Ca(OH)_2$ from JCPDS No. 72-0156; (C) CaO 10'; (D) CaO 10; (E) CaO 08; (F) CaO 05

On the other hand, Figure 1 (d-f) show typical X-ray diffractograms of $Ca(OH)_2$ indicating that its conversion to CaO NPs have not been completely carried out. These results inferred that heating treatment at 400°C was the effective method to convert $Ca(OH)_2$ into CaO NPs, perfectly. Further heat treatment of CaO 10 was the optimum condition to form CaO NPs with high crystallinity. In particular, the crystal size of CaO NPs was calculated using the Debye-Scherrer formula [22] as presented in Equation (3).

$$D = \frac{k\lambda}{\beta \cos\theta} \tag{3}$$

D is the average crystal size (nm), k is Scherrer's constant (0.98), Cu Kα radiation (λ = 1.54060 Å), β is the width of all diffraction peaks (FWHM), and θ refers to the Bragg angle corresponding to the maximum intensity peak. Accordingly, it was found that the average crystal size of CaO NPs at optimum condition was of 4.96 nm.

The FTIR spectra can provide the information of the transformation of $Ca(OH)_2$ into CaO NPs by identification of its functional groups to support the X-Ray diffraction data, since this spectroscopy relies on electromagnetic radiation interference on the surface of the nanoparticles [19]. Figure 2 represented the FTIR spectra of synthesized CaO NPs at various NaOH concentrations, where four typical CaO NPs peaks at wavenumbers 3640, 1400, 860 and 710 cm^{-1} correspond to bending Ca-O, stretching vibration Ca-O and symetric vibration Ca-O-Ca respectively, were clearly observed [23].

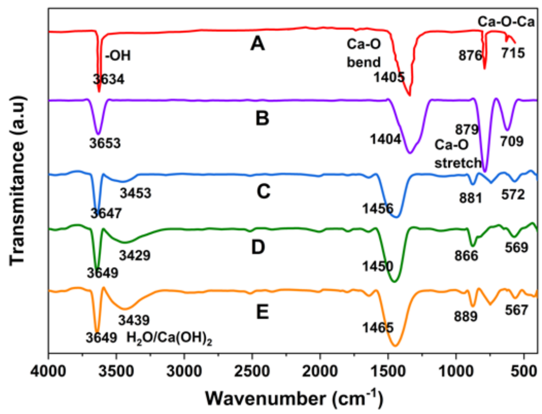

Figure 2. IR Spectra of CaO Nanoparticles: (A) CaO from [23] (B) CaO 10' (C) CaO 10 (D) CaO 08 (E) CaO 05

The second spectrum shows that CaO 10' (temperature 400 + 200°C) has the IR peak most like the reference. The four peaks indicate the presence of Ca-O bonds, Ca-O stretching vibrations and Ca-O-Ca bonds [24]. Meanwhile, spectra 3, 4 and 5 still show the presence of O-H stretching bonds at a wave number of 3400 cm^{-1}, which shows that there are still many O-H groups trapped in these nanoparticles. This indicates that increasing the CaO heating temperature will further optimize the conversion of $Ca(OH)_2$ to CaO. Apart from that, there are CO_3^-, C≡C, C=O and C=C bonds which indicate the presence of $CaCO_3$ due to the absorption of CO_2 particles by CaO in the atmosphere at wave numbers 2500, 2015, 1700 and 1640 cm^{-1}, respectively. This could be due to the transition of carbonate formation during heating or contamination of the sample when it is analyzed using FTIR.

3.2 Morphology

Figure 3 is the result of morphology and texture analysis of CaO nanoparticles using SEM. It was revealed that CaO has a sponge-like morphology with large and small lumps. The bright part is the surface of the CaO nanoparticles which reveals high electron emission when exposed to the electron beam from the SEM instrument [26].

A particle can be called a nanoparticle if its size is 1 to 100 nanometers [27]. The large particle size can be caused by an agglomeration event in the CaO particles, resulting in a larger particle size. The factor that causes this agglomeration may be due to the absence of surfactant in the nanoparticle manufacturing process so that there is no part that can resist agglomeration between particles [28]. However, this agglomeration also reveals the polycrystalline character of CaO nanoparticles which makes them spherical in shape [29]. Comparison of SEM images in Figure 3 between CaO particles with respective NaOH concentrations: 1 M (a, d); 0.8 M (b, e); 0.5M (c, f) a difference can be seen. Figure 3a shows less agglomeration of CaO particles compared to Figures 3b and 3c. This can show that the concentration of NaOH can influence the agglomeration properties of CaO.

In addition, particle size distribution data analysis was carried out using the ImageJ application. The PSD graph in Figure 4 shows a polydispersed distribution curve [30]. In addition, the data shows that only CaO NPs 10 have reached nanometer sizes with an average value of up to 98.1 nm. The size distribution graph for CaO NPs 10 nanoparticles has a positively skewed shape, where the nanoparticle size below 100 nm is more than the size above 100 nm. Meanwhile, in CaO 05 and CaO 08, the particles have not yet reached nano size, with the average particle sizes being 435.7 and 383.9 nm, respectively. The nanoparticle size distribution graphs are both positively skewed and symmetrically normal [31].

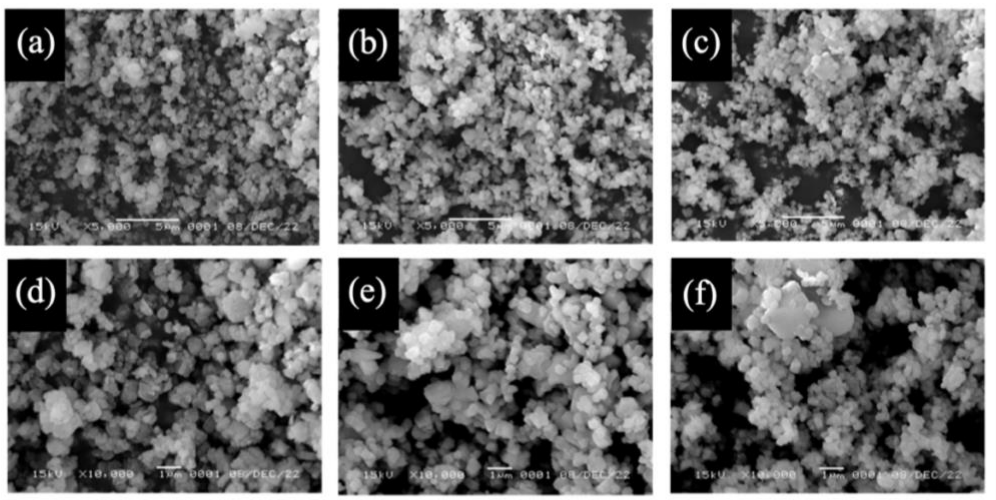

Figure 3. SEM images of (a, d) CaO 10; (b, e) CaO 08; (c, f) CaO 05; (a, b, c) magnification 5,000x; and (d, e, f) magnification 10,000x.

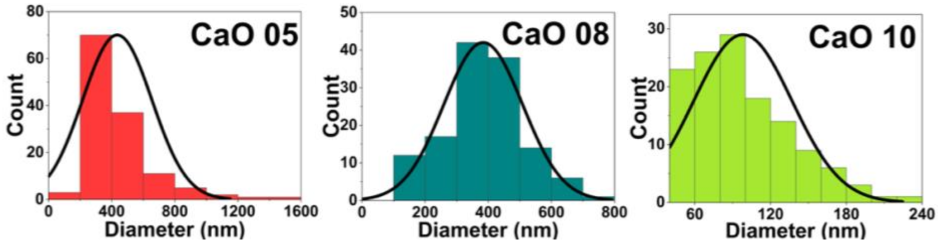

Figure 4. Particle size distribution (PSD) of CaO nanoparticles

3.3. Effect of Base Solution Concentration

The yield of CaO NPs increased with increasing NaOH concentration (Table 1), due to stoichiometry relation of two hydroxyl ion (OH^-) are required to react with calcium ion (Ca^{2+}) to produce calcium hydroxide ($Ca(OH)_2$) precipitate [32]. Sodium ions (Na^+) are more reactive than Ca^{2+} ions due to the electronic configuration of their outer cells. Therefore, Na^+ ions in solution can attract Cl^- ions resulting in precipitated sodium chloride (NaCl) as shown by Equation (5).

$$CaCl_2 + 2NaOH \rightarrow Ca(OH)_2 + 2NaCl \quad (5)$$

The residual NaCl was removed from the $Ca(OH)_2$ precipitate by washing with deionized water. The white precipitate $Ca(OH)_2$ was transformed to calcium oxide (CaO) by furnace at 400°C (Equation (6)).

$$Ca(OH)_{2\,(s,wet)} \rightarrow CaO_{(s)} + H_2O_{(g)} \quad (6)$$

Table 1. CaO NPs yield at various NaOH concentration.

[NaOH] (M)	CaO NPs Yield (%)
0.5	68.27
0.8	74.26
1.0	74.56

3.4 Adsorption Study

3.4.1 Effect of adsorbent dosage to the IC removal percentage

For variations in adsorbent dose, based on Table 2, it can be concluded that the best removal percentage of the CaO nanoparticle dose was at a dose of 10 mg which reached 38% with a Q_e value of 11.53 mg/g. This could be caused by the presence of the adsorbent active site which was able to absorb the whole OH group in indigo carmine dye. So, if the dose is increased, the number of remaining OH groups will decrease [33]. Therefore, in adsorption tests at varying dye solution concentrations and contact times, an adsorbent dose of 10 mg will be used, because it has the best number of active sites.

Table 2. Removal Percentage (%) of CaO Nanoparticles at Varying Adsorbent Doses

Adsorbent dose (mg)	Q_e (mg/g)	%Removal (%)
10	11.526	38
20	4.973	33
30	2.439	24
40	1.566	21

3.4.2 Isotherm Adsorption Study

By varying the adsorbate concentration, the value of the adsorption capacity (Q_e) of nanoparticles was obtained at various concentrations of standard indigo carmine (IC) solution. The greater the IC concentration, the greater the adsorption capacity of CaO nanoparticles.

In this variation, plotting was carried out using adsorption isotherm modeling. In this study, six adsorption isotherm models were used, such as the Langmuir, Freundlich, Temkin, Redlich-Peterson, Sips, and Koble-Corrigan isotherms shown in Figure 5 and Table 3 which were fitted using non-linear equations [34]. From the six models, it was found that the Koble-Corrigan adsorption isotherm model was the best model. with a coefficient of determination (R^2) of 0.99 and a chi-square value of 0.38 (Table 4). The theory of this modeling reveals that the adsorbent has a homogeneous adsorption surface with various active sites to absorb dye molecules. This also proves the existence of an electrostatic force of attraction between the adsorbate (indigo carmine) and the adsorbent (CaO) which supports the previous adsorption mechanism theory [35].

Table 3. Non-linear equations for Langmuir, Freundlich, Temkin, Sips, Redlich-Peterson, and Koble-Carrigan isotherm models [39–43].

Isotherm Model	Non-linier Equation
Langmuir	$Q_e = \frac{Q_0 K_L C_e}{1 + K_L C_e}$ Separation factor: $R_L = \frac{1}{1 + K_L C_0}$
Freundlich	$Q_e = bC_e^{1/n}$
Temkin	$Q_e = \frac{RT}{b}\ln(K_T C_e)$
Sips	$Q_e = \frac{Q_{ms}\alpha_s C_e^{B_s}}{1 + \alpha_s C_e^{B_s}}$
Redlich-Peterson	$Q_e = \frac{K_r C_e}{1 + \alpha C_e^{\beta}}$
Koble-Carrigan	$Q_e = \frac{A_k C_e^p}{1 + B_k C_e^p}$

Apart from that, Table 4 also shows several parameters from other adsorption isotherm modeling which can explain several theories of the adsorption mechanism that occurs in indigo carmine through CaO.

Table 4. Adsorption isotherm modeling parameters

Model	Parameter	Value
Langmuir	Q_0 (mg/g)	41.34489
	K_L (L/mg)	2.7622
	x^2	1.6111
	R_L	0.18
	R^2	0.86808
Freundlich	K_F (L/mg)	0.04702
	n	0.46189
	x^2	1.4766
	R^2	0.87054
Temkin	RT/b	25.60153
	K_T (L/mg)	0.13686
	x^2	1.5528
	R^2	0.87287
Redlich-Peterson	K_r (L/mg)	1.0564
	α (L/mg)	2.23695
	β	0.55328
	x^2	1.4766
	R^2	0.87911
Sips	Q_{ms} (mg/g)	154.77996
	α_s (L/mg)	4.72006
	C_e	155.63474
	β_s	1.00249
	R^2	0.91812
Koble-Corrigan	A_k	1.721
	B_k	6.2434
	p	9.99211
	x^2	0.38459
	R^2	0.99685

In modeling the Langmuir isotherm, an R_L (separation factor) value is obtained with a value of $0 < R_L < 1$. This value reveals that this model is preferred, and the adsorption process occurs in a monolayer manner. In addition, the active site on the adsorbent is homogeneous and the adsorption energy used is constant (does not change) [36].

In modeling the Freundlich isotherm, the value of n is less than one (0.46), so the adsorption process occurs chemically. Meanwhile, the value of 1/n is more than one (2.71), which indicates that the Freundlich modeling theory is less suitable for the indigo carmine adsorption process. by CaO that the process occurs through heterogeneous sites and the energy distribution is not constant. The Temkin isotherm model reveals that the amount of adsorption energy used is 25.6 kJ/mol or more than 8 kJ/mol, which shows that the adsorption process occurs chemically. In this way, Freundlich's theory has been validated by Temkin that this adsorption process occurs chemically [37].

The Redlich and Sips isotherm modeling supports Langmuir theory, that the adsorption process occurs in a monolayer through high concentrations. This is proven by the Redlich β value approaching 1 and the Sips n value more than 1 [38].

3.4.3 Kinetics Adsorption Study

By varying the adsorption contact, the value of the adsorption capacity (Q_t) of the nanoparticles at a certain adsorption time is obtained. The longer the adsorption time, the greater the adsorption capacity of CaO nanoparticles. In this study, the adsorption contact time has not reached the optimum time, which indicates that CaO 10 can still adsorb indigo carmine if the time continues to be added.

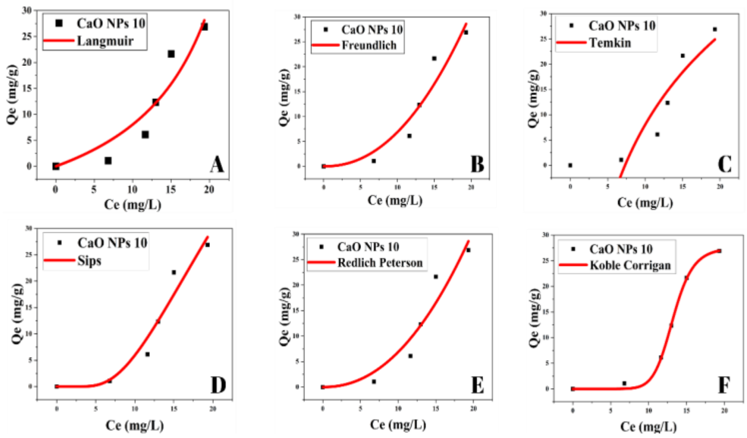

Figure 5. Adsorption isotherm modeling plotting (A) Langmuir; (B) Freundlich; (C) Temkin; (D) Sips; (E) Redlich-Peterson; and (F) Koble-Corrigan

In this study, plotting was also carried out on various adsorption kinetic models such as pseudo first order, pseudo second order, and intra-particle diffusion which are shown in Figure 6. Based on the parameters of the three adsorption kinetic models (Table 5), it was found that the pseudo first order and pseudo second order models orders have a coefficient of determination (R^2) of 0.99. However, pseudo second order has a calculated Q_e value of 11.041 mg/g which is closer to the experimental Q_{max} value of 5.42 mg/g as shown in Table 6. This indicates that the adsorption process depends on the adsorption capacity [44]. Meanwhile, in pseudo first order, the calculated Q_e value is -86.21 mg/g. The Q_e value is negative, which indicates that this modeling adsorption process will be difficult to carry out due to the presence of lateral repulsion forces in the adsorption process being carried out [45].

The parameter data from the Intraparticle Diffusion model shows a K_i value > 0, namely 0.63, indicating that the adsorption process of indigo carmine dye occurs through intra-particle diffusion through the pores in CaO nanoparticles [46]. The K_i value < 1 indicates that the adsorption process does not only occur intraparticles but also occurs externally [47].

Table 5. Non-linear equations for pseudo first order, pseudo second order, and intra-praticle diffusion adsorption kinetic models

Kinetic Model	Non-linier	Ref.
Pseudo first order	$Q_t = Q_e(1 - e^{-k_1 t})$	[44]
Pseudo second order	$Q_t = \dfrac{Q_e^2 k_2 t}{1 + Q_e k_2 t}$	
Intra-particle diffusion	$Q_t = K_i t^{0.5} + C$	

Table 6. Adsorption kinetic modeling parameters

Model	Parameter	Value
Pseudo first order	Q_e (mmol g^{-1})	-86.21102
	k_1 (min^{-1})	-0.00121
	R^2	0.99765
Pseudo second order	Q_e (mmol g^{-1})	11.041
	k_2 (g $mmol^{-1}$ min^{-1})	8.7559
	R^2	0.99749
Intra-particle diffusion	K_i (mmol g^{-1} $min^{-0.5}$)	0.63478
	C	3.889
	R^2	0.85959

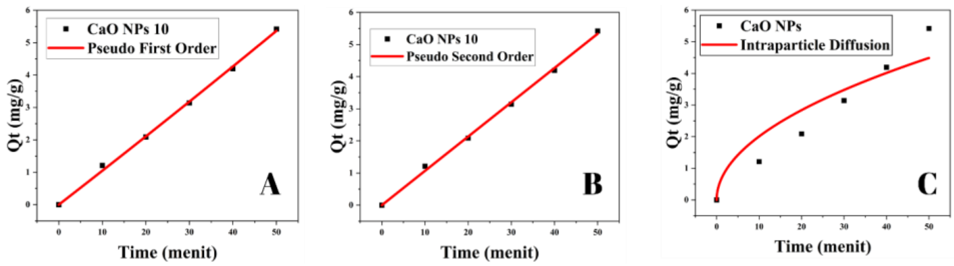

Figure 6. Modeling of CaO nanoparticle adsorption kinetics (A) pseudo first order; (B) pseudo second order, and (C) intraparticle diffusion

4 Conclusion

CaO nanoparticles were successfully synthesized using the coprecipitation method at an optimum concentration of 1 M NaOH and a heating temperature of 400±200°C. Characterization of crystallinity, functional groups, structure, and morphology confirmed the formation of CaO nanoparticles. Adsorption studies also showed that CaO nanoparticles can optimally adsorb indigo carmine (10 mg, 100 ppm, and 50 minutes). The Koble-Carrigan adsorption isotherm model was found to be the most suitable, with an R^2 value of 0.99 and a chi-square value of 0.39. Meanwhile, the pseudo-second-order model was the best fit for adsorption kinetics, with an R^2 value of 0.99.

Acknowledgement

We gratefully acknowledge the excellent supports provided by Ministry of Education, Culture, Research and Technology of Indonesia through World Class Professor (WCP) grant (2808/E4/DT/ 2023) and Indonesia University of Education through Indonesia Research Collaboration (RKI) Scheme-C by World Class University (WCU) (788/UN40.LP/PT.01.03 /2024), and International Research Collaboration (327/UN40.LP/PT.01.03/2024) grants.

References

[1] Neppolian, B., Choi, H.C., Sakthivel, S., Arabindoo, B. and Murugesan, V. 2002. Solar/UV-induced photocatalytic degradation of three commercial textile dyes. *Journal of Hazardous Materials*, Elsevier. 89 (2–3) 303–17. 10.1016/S0304-3894(01)00329-6

[2] Provinsi DKI Jakarta, B. 2017. Data BPS Provinsi DKI Jakarta. Mahendra ,Sri. p. 149–59.

[3] Holkar, C.R., Jadhav, A.J., Pinjari, D. V., Mahamuni, N.M. and Pandit, A.B. 2016. A critical review on textile wastewater treatments: Possible approaches. *Journal of Environmental Management*, Elsevier. 182 351–66. 10.1016/j.jenvman.2016.07.090

[4] Silveira, E., Marques, P.P., Silva, S.S., Lima-Filho, J.L., Porto, A.L.F. and Tambourgi, E.B. 2009. Selection of Pseudomonas for industrial textile dyes decolourization. *International Biodeterioration and Biodegradation*, Elsevier. 63 (2) 230–5. 10.1016/j.ibiod.2008.09.007

[5] Dellamatrice, P.M., Silva-Stenico, M.E., Moraes, L.A.B. de, Fiore, M.F. and Monteiro, R.T.R. 2017. Degradation of textile dyes by cyanobacteria. *Brazilian Journal of Microbiology*, SciELO Brasil. 48 (1) 25–31. 10.1016/j.bjm.2016.09.012

[6] Choi, K.Y. 2021. Discoloration of indigo dyes by eco-friendly biocatalysts. *Dyes and Pigments*, Elsevier. 184 108749. 10.1016/j.dyepig.2020.108749

[7] Ruzicka, O. and Safira, L. 2014. Aplikasi Fotokatalis Tio2 Pada Degradasi Limbah Cair Zat Warna Tekstil. *Lomba Karya Ilmiah Sumber Daya Air Tahun*,.

[8] El-Kammah, M., Elkhatib, E., Gouveia, S., Cameselle, C. and Aboukila, E. 2022. Enhanced removal of Indigo Carmine dye from textile effluent using green cost-efficient nanomaterial: Adsorption, kinetics, thermodynamics and mechanisms. *Sustainable Chemistry and Pharmacy*, Elsevier. 29 100753. 10.1016/j.scp.2022.100753

[9] Kumari, P., Alam, M. and Siddiqi, W.A. 2019. Usage of nanoparticles as adsorbents for waste water treatment: An emerging trend. *Sustainable Materials and Technologies*, Elsevier. 22 e00128. 10.1016/j.susmat.2019.e00128

[10] Kavithayeni, V., Geetha, K. and Akash Prabhu, S. 2019. A review on dye reduction mechanism using nano adsorbents in waste water. *International Journal of Recent Technology and Engineering*, 7 (6) 332–9.

[11] Theodore, L. and Kunz, R.G. 2005. Nanotechnology: Environmental Implications and Solutions. Nanotechnology: Environmental Implications and Solutions. John Wiley & Sons. 10.1002/0471711705

[12] Madhusudhana, N., Yogendra, K. and Mahadevan, K.M. 2012. Photocatalytic Degradation of Violet GL2B Azo dye by using Calcium Aluminate Nanoparticle in presence of Solar light. *Research Journal of Chemical Sciences*, 2 (5) 72–7.

[13] Yousefi-Limaee, N., Ghahari, M., Seifpanahi-Shabani, K., Naeimi, A. and Ghaedi, S. 2023. Evaluation of Adsorptive Efficiency of Calcium Oxide Nanoparticles for the Elimination of Cationic Dyes: Combustion Synthesis, Adsorption Study and Numerical Modeling. *Progress in Color, Colorants and Coatings*, Institute for Color Science and Technology (ICST). 16 (1) 1–20. 10.30509/pccc.2022.166898.1136

[14] Geethakarthi, A. and Hemapriya, S. 2022. Degradation of an Acid Dye using Calcium Oxide Extracted from Waste Egg Shells. *AIP Conference Proceedings*, AIP Publishing. 10.1063/5.0109148

[15] Thakur, S., Singh, S. and Pal, B. 2022. Superior adsorptive removal of brilliant green and phenol red dyes mixture by CaO nanoparticles extracted from egg shells. *Journal of Nanostructure in Chemistry*, Springer. 12 (2) 207–21. 10.1007/s40097-021-00412-x

[16] Ma, X., Yuan, W., Bell, S.E.J. and James, S.L. 2014. Better understanding of mechanochemical reactions: Raman monitoring reveals surprisingly simple 'pseudo-fluid' model for a ball milling reaction. *Chemical Communications*, Royal Society of Chemistry. 50 (13) 1585–7. 10.1039/c3cc47898j

[17] Donkadokula, N.Y., Kola, A.K., Naz, I. and Saroj, D. 2020. A review on advanced physico-chemical and biological textile dye wastewater treatment techniques. *Reviews in Environmental Science and Biotechnology*, Springer. 19 (3) 543–60. 10.1007/s11157-020-09543-z

[18] Kurnia, I., Karnjanakom, S., Irkham, I., Haryono, H., Situmorang, Y.A., Indarto, A. et al. 2022. Enhanced adsorption capacity of activated carbon over thermal oxidation treatment for methylene blue removal: kinetics, equilibrium, thermodynamic, and

reusability studies. *RSC Advances*, Royal Society of Chemistry. 13 (1) 220–7. 10.1039/d2ra06481b

[19] Ramola, B. and Joshi, N.C. 2019. Green Synthesis, Characterisations and Antimicrobial Activities of CaO Nanoparticles. *Oriental Journal of Chemistry*, Oriental Scientific Publishing Company. 35 (3) 1154–7. 10.13005/ojc/350333

[20] Aqliliriana. 2015. Preparation And Characterization Of Modified Calcium Oxide From Natural Sources And Their Application In The Transesterification Of Palm Oil. *International Journal of Scientific & Technology Research*, 4 (8) 168–75.

[21] Tanpure, S., Ghanwat, V., Shinde, B., Tanpure, K. and Lawande, S. 2022. The Eggshell Waste Transformed Green and Efficient Synthesis of K-Ca(OH)2 Catalyst for Room Temperature Synthesis of Chalcones. *Polycyclic Aromatic Compounds*, Taylor & Francis. 42 (4) 1322–40. 10.1080/10406638.2020.1776740

[22] Habte, L., Shiferaw, N., Mulatu, D., Thenepalli, T., Chilakala, R. and Ahn, J.W. 2019. Synthesis of nano-calcium oxide from waste eggshell by sol-gel method. *Sustainability*, MDPI. 11 (11) 3196.

[23] Garba, A.A. and Usman, B. 2021. OPTIMIZATION AND EVALUATION OF BIODIESEL QUALITY PRODUCED FROM CATTLE FAT USING CaO/AhO3 AS CATALYST. *Moroccan Journal of Chemistry*, 9 (1) 132–41. 10.48317/IMIST.PRSM/morjchem-v9i1.17260

[24] Anantharaman, A. and George, M. 2016. Green Synthesis of Calcium Oxide Nanoparticles and Its Applications. *Journal of Engineering Research and Application WwwIjeraCom*, 6 (10) 27–31.

[25] Khachani, M., El Hamidi, A., Halim, M. and Arsalane, S. 2014. Non-isothermal kinetic and thermodynamic studies of the dehydroxylation process of synthetic calcium hydroxide Ca(OH)2. *Journal of Materials and Environmental Science*, Citeseer. 5 (2) 615–24.

[26] Kasirajan, R., Bekele, A. and Girma, E. 2022. Adsorption of lead (Pb-II) using CaO-NPs synthesized by solgel process from hen eggshell: Response surface methodology for modeling, optimization and kinetic studies. *South African Journal of Chemical Engineering*, South African Institution of Chemical Engineers (SAIChE). 40 (1) 209–29. 10.1016/j.sajce.2022.03.008

[27] Vert, M., Doi, Y., Hellwich, K.H., Hess, M., Hodge, P., Kubisa, P. et al. 2012. Terminology for biorelated polymers and applications (IUPAC recommendations 2012). *Pure and Applied Chemistry*, De Gruyter. 84 (2) 377–410. 10.1351/PAC-REC-10-12-04

[28] Naullage, P.M., Bertolazzo, A.A. and Molinero, V. 2019. How Do Surfactants Control the Agglomeration of Clathrate Hydrates? *ACS Central Science*, ACS Publications. 5 (3) 428–39. 10.1021/acscentsci.8b00755

[29] Mirghiasi, Z., Bakhtiari, F., Darezereshki, E. and Esmaeilzadeh, E. 2014. Preparation and characterization of CaO nanoparticles from Ca(OH)2 by direct thermal decomposition method. *Journal of Industrial and Engineering Chemistry*, Elsevier. 20 (1) 113–7. 10.1016/j.jiec.2013.04.018

[30] Shin, W.G., Pui, D.Y.H., Fissan, H., Neumann, S. and Trampe, A. 2007. Calibration and numerical simulation of Nanoparticle Surface Area Monitor (TSI Model 3550 NSAM). *Journal of Nanoparticle Research*, Springer. 9 (1) 61–9. 10.1007/s11051-006-9153-y

[31] Zhdanov, V.P. 2008. Kinetics of migration and coalescence of supported nm-sized metal particles. *Surface Review and Letters*, World Scientific. 15 (3) 217–20. 10.1142/S0218625X08011263

[32] Khine, E.E., Koncz-Horvath, D., Kristaly, F., Ferenczi, T., Karacs, G., Baumli, P. et al. 2022. Synthesis and characterization of calcium oxide nanoparticles for CO2 capture. *Journal of Nanoparticle Research*, Springer. 24 (7) 139. 10.1007/s11051-022-05518-z

[33] Subramani, A.K., Byrappa, K., Ananda, S., Lokanatha Rai, K.M., Ranganathaiah, C. and Yoshimura, M. 2007. Photocatalytic degradation of indigo carmine dye using TiO2 impregnated activated carbon. *Bulletin of Materials Science*, Springer. 30 (1) 37–41. 10.1007/s12034-007-0007-8

[34] Vitek, R. and Masini, J.C. 2023. Nonlinear regression for treating adsorption isotherm data to characterize new sorbents: Advantages over linearization demonstrated with simulated and experimental data. *Heliyon*, 9 (4) e15128. 10.1016/j.heliyon.2023.e15128

[35] Muangrak, W., Thouchprasitchai, N., Phongboonchoo, Y. and Pongstabodee, S.

2020. Dual functional composite of montmorillonite-rich/chitosan (Mcc) for decolorizing the water used in joss paper process: Thermodynamic, isotherm, and kinetic studies. *Applied Sciences (Switzerland)*, MDPI. 10 (21) 1–16. 10.3390/app10217493

[36] Kalam, S., Abu-Khamsin, S.A., Kamal, M.S. and Patil, S. 2021. Surfactant Adsorption Isotherms: A Review. *ACS Omega*, ACS Publications. 6 (48) 32342–8. 10.1021/acsomega.1c04661

[37] Ayawei, N., Ebelegi, A.N. and Wankasi, D. 2017. Modelling and Interpretation of Adsorption Isotherms. *Journal of Chemistry*, Hindawi. 2017. 10.1155/2017/3039817

[38] Ramesh, T.N., Kirana, D.V., Ashwini, A. and Manasa, T.R. 2017. Calcium hydroxide as low cost adsorbent for the effective removal of indigo carmine dye in water. *Journal of Saudi Chemical Society*, Elsevier. 21 (2) 165–71. 10.1016/j.jscs.2015.03.001

[39] Afif, A., Rahman, S.M., Tasfiah Azad, A., Zaini, J., Islam, M.A. and Azad, A.K. 2019. Advanced materials and technologies for hybrid supercapacitors for energy storage – A review. *Journal of Energy Storage*, Elsevier. 25 100852. 10.1016/j.est.2019.100852

[40] Foo, K.Y. and Hameed, B.H. 2010. Insights into the modeling of adsorption isotherm systems. *Chemical Engineering Journal*, Elsevier. 156 (1) 2–10. 10.1016/j.cej.2009.09.013

[41] Saadi, R., Saadi, Z., Fazaeli, R. and Fard, N.E. 2015. Monolayer and multilayer adsorption isotherm models for sorption from aqueous media. *Korean Journal of Chemical Engineering*, Springer. 32 (5) 787–99. 10.1007/s11814-015-0053-7

[42] Liu, Q.S., Zheng, T., Wang, P., Jiang, J.P. and Li, N. 2010. Adsorption isotherm, kinetic and mechanism studies of some substituted phenols on activated carbon fibers. *Chemical Engineering Journal*, Elsevier. 157 (2–3) 348–56. 10.1016/j.cej.2009.11.013

[43] Alahmadi, S., Mohamad, S. and Maah, M.J. 2014. Comparative study of tributyltin adsorption onto mesoporous silica functionalized with calix[4]arene, p-tert-butylcalix[4]arene and p-sulfonatocalix[4]arene. *Molecules*, MDPI. 19 (4) 4524–47. 10.3390/molecules19044524

[44] Sen Gupta, S. and Bhattacharyya, K.G. 2011. Kinetics of adsorption of metal ions on inorganic materials: A review. *Advances in Colloid and Interface Science*, Elsevier. 162 (1–2) 39–58. 10.1016/j.cis.2010.12.004

[45] Timothy, E., Khaled, E. and Erric, E. 2012. Kinetics, equilibrium, and isotherm of the adsorption of chlorine by TDRP. *Tenside, Surfactants, Detergents*, Elsevier. 49 (5) 376–81. 10.3139/113.110205

[46] Campos, N.F., Barbosa, C.M.B.M., Rodríguez-Díaz, J.M. and Duarte, M.M.M.B. 2018. Removal of naphthenic acids using activated charcoal: Kinetic and equilibrium studies. *Adsorption Science and Technology*, SAGE Publications Sage UK: London, England. 36 (7–8) 1405–21. 10.1177/0263617418773844

[47] Priyantha, N., Lim, L.B.L. and Kh, M. 2013. Dragon Fruit Skin As a Potent Removal of M. *Journal of Applied Sciences in Environmental Sanitation*, 8 (3) 179–88.